

Geometry and Properties of the Excavation-Induced Fractures at the Meuse/Haute-Marne URL Drifts

G. Armand · F. Leveau · C. Nussbaum ·
R. de La Vaissiere · A. Noiret · D. Jaeggi ·
P. Landrein · C. Righini

Received: 12 November 2012 / Accepted: 16 November 2012 / Published online: 8 January 2013
© Springer-Verlag Wien 2013

Abstract The performance and safety assessment and technology demonstration are the main objectives of research programs for feasibility studies for deep geological repository of radioactive waste. In this context, the French national radioactive waste management agency (ANDRA) started to develop the Meuse/Haute-Marne underground research laboratory (URL) at Bure, nearly 300 km East of Paris. The host formation consists of a Callovo-Oxfordian claystone found between 420 and 550 m below ground, overlain and underlain by poorly permeable carbonate formations. One of the major concerns related to performance assessment is the excavation-induced fractures which may provide groundwater preferential pathway for radionuclide migration. The extent of the fractures possibly acting significantly in the radionuclide migration is known as the excavation damaged zone (EDZ). A scientific study on the EDZ characterization is performed at the main level of the URL (−490 m). Observations such as structural analysis on core, overcored resin-filled samples, geological survey of the drift face and sidewalls, were made to better understand the fracture network characteristics, extent and its generation. Pulse and constant head test hydraulic conductivity measurements were performed with multi packer system to

estimate the extension of the EDZ hydraulic conductivity. Fractures exhibited high transmissivity near the excavation walls, but farther from the excavation walls, shear fractures showed hydraulic conductivity values reflecting values of undisturbed or slightly disturbed rock mass condition. The major findings in terms of geometry and properties of excavation-induced fractures are discussed in detail in this paper. For example, it is observed that the shape of the fracture network depends on the orientation of the drift in relation to the orientation of the in situ stress field.

Keywords Excavation damaged zone (EDZ) · Excavation-induced fractures · Claystone · Hydraulic conductivity · Underground research laboratory · Deep geological repository

1 Introduction

Excavation of underground drifts generally causes damage to the rock in the vicinity of the openings. The level of damage depends on various factors such as the rock properties, in situ stress field, geometry of the openings, excavation method and time. Stress redistribution could result in unloading, joints and shear fractures to appear in the vicinity of the openings, thereby affecting the hydro-mechanical properties of the rock.

When considering the long-term safety of nuclear waste in a repository, question arises about the fractures ability around the galleries to provide a preferential pathway for groundwater and radionuclides migration.

Earlier researchers used both the terms “disturbed zone” (Pusch and Stanfors 1992) and “damaged zone”. Fairhurst and Damjanac (1996) noted that “excavation damaged zone (EDZ) and disturbed rock zone (DRZ) are used

G. Armand (✉) · R. de La Vaissiere · A. Noiret · P. Landrein ·
C. Righini
ANDRA Laboratoire de Meuse/Haute-Marne, Route
Départementale 960, 55290 Bure, France
e-mail: gilles.armand@andra.fr

F. Leveau
GEOTER, Route Départementale 960, 55290 Bure, France

C. Nussbaum · D. Jaeggi
SWISSTOPO, Fabrique de Chaux,
2882 St-Ursanne, Switzerland

synonymously to describe the region of rock adjacent to an underground opening that has been significantly damaged or disturbed due to the redistribution of in situ stresses". Emsley (1997) was the first who made a clear distinction between disturbed and damaged zone, by defining the excavation damaged zone as "a damaged zone closest to the drift wall dominated by changes in material properties which are mainly irreversible" and the Excavation Disturbed Zone as "a disturbed zone outside the damaged zone dominated by changes in stress state and hydraulic head and where changes in rock properties are small and mainly reversible and it is considered that there are no, or insignificant, material property changes".

An international consensus (Tsang et al. 2005) defined an excavation damaged zone (EDZ) as "a zone in which hydromechanical and geochemical modifications induce significant changes in flow and transport properties. These changes can, for example, include one or more orders of magnitude increase in flow permeability". This is obviously important only if the hydraulic pathway provided by the EDZ will be greater than a pathway provided through the backfilled excavations or along the interface between the backfill and the rock. This definition is used in this paper.

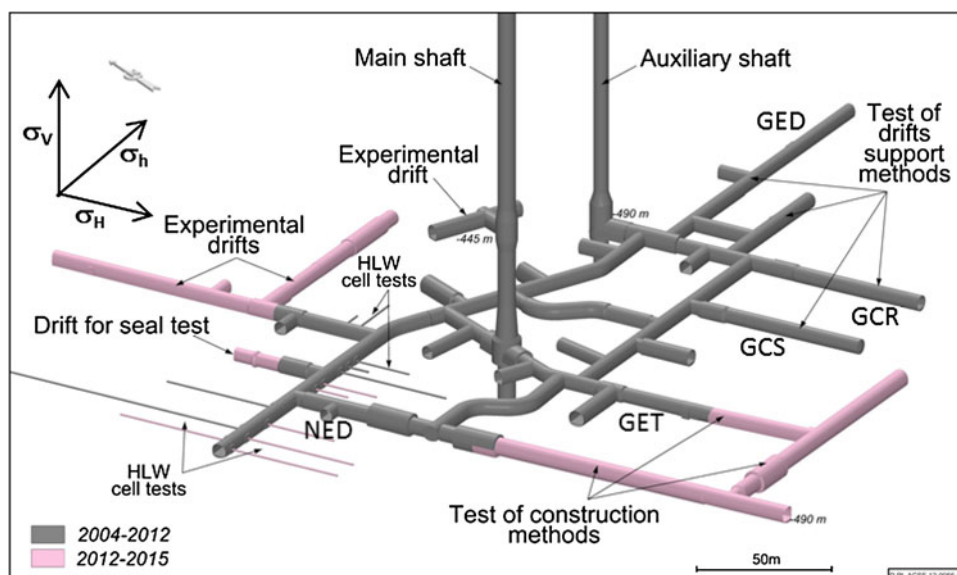
Clay formations in their natural state exhibit very favorable confining conditions for repository of radioactive waste because they generally have a very low hydraulic conductivity, small molecular diffusion and significant retention capacity for radionuclides. Nevertheless, one concern regarding waste disposal is that the associated disturbance and damage created in the area around these excavations might change the favorable properties of such formations and the host rock might lose part of its barrier

function and thus negatively impact the repository performance. To demonstrate the feasibility of a radioactive waste repository in a claystone formation, the French national radioactive waste management agency (ANDRA) started in 2,000 to build the Bure underground research laboratory (URL) at nearly 300 km East of Paris. The URL host formation consists of a Callovo-Oxfordian argillite found between 420 and 550 m below ground overlain and underlain by poorly permeable carbonate formations.

The main objective of the first research phase was to characterize the confining properties of the clay through in situ hydrogeological tests, chemical measurements and diffusion experiments and to demonstrate that the construction and operation of a geological repository would not introduce pathways for radionuclides migration (Delay et al. 2007). One of the main purposes of geo-mechanical experimental program was to collect data on features, extension and hydraulic properties of the EDZ for supporting evidence required for the repository safety assessment (Blümling et al. 2007). The excavation worksite in the host formation is a scientific experimentation in itself to characterize the impact of excavation to understand the hydro-mechanical behavior of the claystone and to study the excavation damaged zone (EDZ). The experimental drifts network is located at the main level (−490 m) and at −445 m of the URL (Fig. 1).

During the last decade, a large number of experiments in different URLs were dedicated to the study of the EDZ in clay formations. Studies have been performed both in indurated clay formations, like the Opalinus clay (Martin et al. 2002; Schuster et al. 2001) at Mont Terri (Switzerland), and in plastic clay formations, like the Boom clay at Mol (Belgium) (Bastiaens et al. 2007). These studies have

Fig. 1 Meuse/Haute-Marne URL drifts network, (grey already excavated, pink to be excavated)



developed several methods to assess the extension of the EDZ. No method achieves a full understanding of the EDZ and the foremost difficulty is to define exactly what EDZ with respect to potential significant changes in flow and transport properties of the rock.

In the Meuse/Haute-Marne URL, an extensive program of experimental studies was planned to characterize the response of the host rock to different shaft and drift excavation/construction methods and EDZ. Numerous experiments and direct measurements were performed in the laboratory drifts at -445 m (excavated from the main shaft in 2004) and in drifts at -490 m (excavated from auxiliary shaft in 2005) and also during the excavation and construction of the main shaft between -445 and -490 m. These various configurations gave insight of the influence of the structure geometry, the natural stress state and the rock mechanical properties. Furthermore, understanding the impact of support and excavation methods on the hydro-mechanical behavior of the drift in the short and long term is necessary to optimize the design of the drift support for the repository.

At the main level of the laboratory (at -490 m) no natural joints and no faults were observed in the cores of deep boreholes drilled from the surface or during excavation of the shafts and drifts. During construction of the first drift from the auxiliary shaft at the main level of the URL, large stress-induced fractures (chevron type) appeared on the working face (Fig. 2), but only some scattered short cracks were observed in the drift at -445 m. The difference is related to a higher calcite content at -445 m than at -490 m resulting in a claystone strength up to 10 MPa higher.

The paper describes different experimental methods carried out to characterize the excavation-induced fractures network observed at the main level of the Meuse/Haute-

Marne URL and discusses the EDZ extent versus the fracture network.

2 The Meuse/Haute-Marne Underground Research Laboratory

2.1 Callovo-Oxfordian Claystone

Different laboratory tests have been conducted on core samples to obtain the hydro-mechanical properties of the claystone. Mineralogical composition varies slightly within the stratigraphic levels. At the -490 m level, mineralogical study showed a rather homogeneous composition of tectosilicates (20 %), carbonates (20–25 %) and clay minerals (50–55 %) together with subordinate pyrite and iron oxides (3 %). The clay minerals composition is relatively constant at 55 % I/S (illite–smectite interstratified minerals), 30 % illite and 15 % kaolinite and chlorite. Due to a very small mean pore diameter (~ 0.02 μm), the claystone has a low permeability ($\sim 5 \times 10^{-20}$ to 5×10^{-21} m^2) and its average porosity is between 14 and 21 % and equal to 18 ± 1 % at the main level of the URL. Natural water content of core samples ranges between 5 and 8 %. Pore pressure at the main level (-490 m) is around 4.7 MPa.

Table 1 represents the Callovo-Oxfordian argillite mechanical characteristics. Sedimentation has led to a slightly anisotropic behavior of the argillite not taken into account in Table 1. From compressive and shear wave measurements on cubic samples, the anisotropy ratio of the dynamic Young Modulus is around 1.3.

2.2 Virgin Stress State

Anisotropic stress state of the claystone was determined by Wileveau et al. (2007). The major stress (σ_H) is



Fig. 2 View of a front with chevron fractures at the main level (from Geoter)

Table 1 Main characteristics of the Callovo-Oxfordian claystone at the main level of the URL

Rock parameter	Ind	Value
Density	ρ	2.39 g/cm^3
Porosity	n	18 ± 1 %
Young modulus	E	4000 ± 1470 MPa
Poisson ratio	ν	0.29 ± 0.05
Uniaxial compressive strength	UCS	21 ± 6.8 MPa
Hoek–Brown criteria		
S		0.43
m		2.5
σ_c (MPa)		33.5
Intrinsic permeability	k	5×10^{-20} m^2
Water content	w	7.2 ± 1.4 %

horizontally oriented at NE150°. The vertical stress (σ_v) is nearly equal to the horizontal minor one (σ_h):

$$\sigma_v = \rho g Z \text{ and } \sigma_h \approx \sigma_v$$

with Z the depth, ρ the density and g the gravity.

The ratio σ_H/σ_h is close to 1.3 and varying of magnitude with depth and the rheological characteristics of the respective layers.

2.3 Excavation and Support Methods of URL Drift Network

At the main level of the URL (Fig. 1), the orientation of the experimental drifts has been determined according to the orientation of in situ stress field. Initial excavation was carried out by pneumatic hammering technique. After a maximum progression of 2 m, excavated zone was supported immediately by bolts, sliding arches and 10 cm thick layer of shotcrete was set in place. Another excavation technique with a road header has been used with stiff and flexible support (drift GET, GCS & GCR). A tunnel boring machine (TBM) will be tested with segments emplacement technique in 2013. All new experimental drifts are instrumented in order to measure the short- and long-term hydro-mechanical behavior of the EDZ. This will also assist in understanding the impact of different support stiffness on the rock mass behavior in the long term.

ANDRA planned to compare hydro-mechanical behavior around two experimental drifts (GCS and GCR) parallel to the major horizontal stress (Armand et al. 2011). Those 60 m long drifts were excavated with a road header and with two different support systems. The circular section of these drifts has a 2.6 m radius. This excavation method resulted in an average excavated radius of 2.7 m vertically and up to 3.0 m horizontally. The spans of the excavation are mainly 1.2 m long and are immediately covered with a 3 to 5 cm thick fiber shotcrete.

The support of the GCS drift is ensured by a 18 cm thick fiber reinforced shotcrete shell, interrupted by 12 yieldable concrete props (hiDCon[®]) and completed by a crown of 12 HA25 radial bolts of 3 m length every meter. Eleven rock bolts, 12 m long, are placed at the front face every 6 m. A complete description of the work can be found in Bonnet-Eymard et al. (2011). The GCR drift is experimented with a stiff concrete support poured a few months after its excavation in order to stop deformations.

The comparison will enable to understand relationship between rock deformation in the EDZ and support loading. The experiments will also provide a database to check the ability and capacity of numerical models to reproduce and simulate the hydro-mechanical behavior of the rock mass. Martin et al. (2010) described the work for the other drifts

with a horse shoe section with a counter vault. This paper mainly discusses the experiments and observations performed in GET and GCS drifts parallel to the horizontal major stress and it also gives an insight on drift GED parallel to the horizontal minor stress.

3 Methods of Characterization of the Induced Fractures Network

Armand et al. (2007) recall the common measuring methods used to assess the EDZ extension around drifts at the main level of the Meuse/Haute-Marne URL and also around a specific sealing experiment for cutting off the EDZ hydraulic connectivity:

- Structural analysis of the core samples and 3D analysis to characterize the types of fracture and to define the fracture density according to depth,
- Geological survey of the drift face and sidewalls,
- Seismic measurements: interval velocity measurements to study the evolution of P and S wave velocities according to the distance from the drift wall in single or cross hole (Schuster et al. 2001) or seismic refraction (these measurements are not discussed in this paper),
- Permeability measurements carried out through gas and/or hydraulic tests to assess the EDZ hydraulic conductivity with time and the degree of saturation of argillites (Bossart et al. 2002), and
- Overcoring of resin-filled EDZ fractures (Bossart et al. 2002), a method to efficiently visualize and measure fractures.

3.1 Structural Analysis

Two methods have been used to study excavation-induced fractures:

- 3D scan measurement to determine strike, dip and sense of fractures located on faces and walls of the drift.
- Geological survey performed on cores from boreholes around the experimental drifts.

3.1.1 3D Scanner

Detailed geological survey with a 3D scan was conducted every meter in the first 3 m of an excavation and then at 5 m interval. The survey was conducted in two steps (Fig. 3): (1) A total station measures about one million topographic georeferenced points on the excavated faces and walls of the drift with a resolution of 5 mm, and (2) a 3D model of the excavation is established. The drift excavation-induced structures are identified and mapped,

observable slickensides measured and fractures classified according to their specific typology. The dip and the strike of each fracture plan are automatically calculated by the 3D model. This method allows to generate a significant database on fracture types, orientation in a real 3D frame and to produce statistical data on the fracture pattern.

3.1.2 On Drilled Cores

Since 2005, core samples from nearly 400 horizontal, vertical and oblique boreholes drilled in the URL drifts were investigated. More than 4,000 excavation-induced fractures were studied and no fault or natural fracture were identified in the cores. Some fractures induced by drilling were identified and were not taken into account during the analysis.

Cores are reconstituted and oriented based on position in the borehole and the nearly horizontal stratification in the drifts. The three possible cases are:

- Vertical boreholes: the nearly horizontal stratification is obvious but the orientation cannot be determined. Only the dip of fractures can be measured. A lesser quality rating of 3 is attributed to this type of measurement.
- Horizontal boreholes: orientation relative to north is obvious but the stratification is not observed. Fractures measurement consistent with observations in drifts is selected and a medium quality rating of 2 is given to this type of measurement.
- Oblique boreholes: the orientation and stratification are certain and a good quality rating of 1 is given to this type of measurement.
- When oriented borehole images are available, cores are clearly oriented and a quality rating of 1 is given to the measurement.

All fractures and slickensides are classified according to two types of breaks (shear fracture or unloading tensile

fractures, Fig. 4) and a criterion of uncertainty is defined depending on the orientation quality:

- Quality 1: Orientation of the core is certain. Fracture measurements are certain.
- Quality 2: Orientation of the core is uncertain with two possibilities.
- Quality 3: Orientation of the core is not determined. Only the depth and dip of fractures can be measured.

3.2 Resin Injection

The principle of resin injection for studying the fractured rock mass in a borehole wall was first developed and applied by Moeri and Bossart (1999) and is illustrated in Bossart et al. (2002). A “Sika Injection 26” doped with a fluorescent dye (fluorescein) was used as a resin. Resin was filled into a PVC-liner, which was inserted into the pressure vessel (Fig. 5) with two lines; one for pressurization and the other for resin injection. By monitoring the manometer, pressure in the pressure vessel is controlled and can be recorded. Another line is for injecting resin into a borehole. The injection pressure is limited, in order to prevent the creation of new fractures or to enlarge pre-existing fractures. The maximal injection pressure in this case was limited to 12 bars to have sufficient pressure gradients and to remain under estimated stress around the drift. In some cases, the pressure had reached 14 bars. Opening of the fractures near the wall due to the resin injection pressure remains possible with the applied pressure.

The injection borehole has a diameter of 42 mm. For boreholes longer than 3 m, resin injection was performed in two phases to guarantee complete impregnation all along the borehole, without any pressure drop during the injection phase. The injection strategy for 4.5 m long sub-horizontal boreholes is illustrated in Fig. 6. The first packer is set at 3.0 m, to seal the interval from 3 to 4.5 m. The

Fig. 3 3D scan structural survey

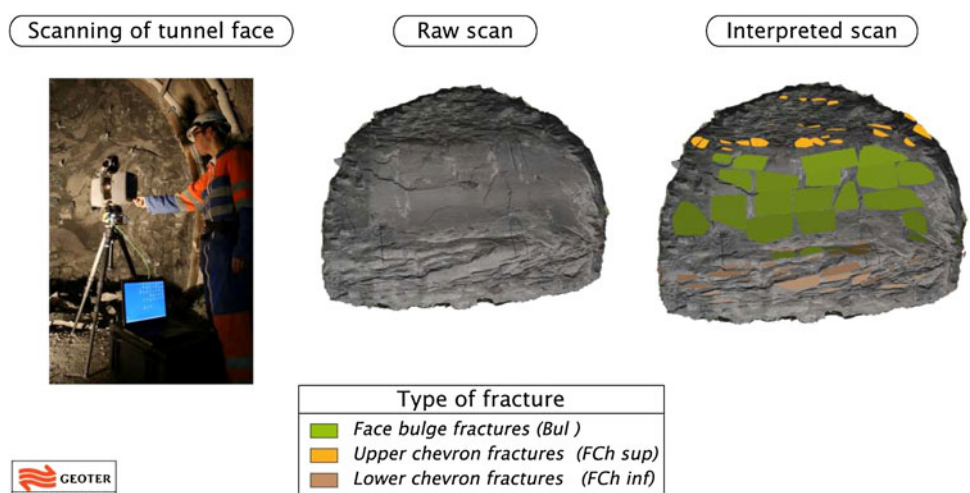


Fig. 4 Observed drill core structures: shear and extensional fractures

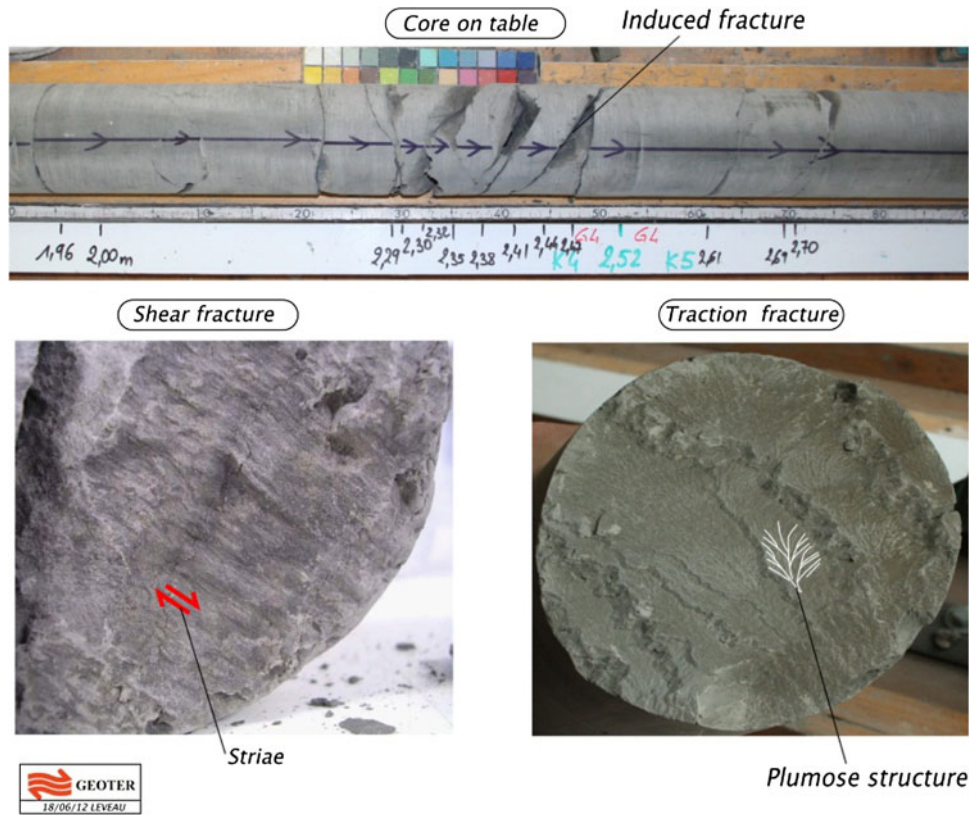
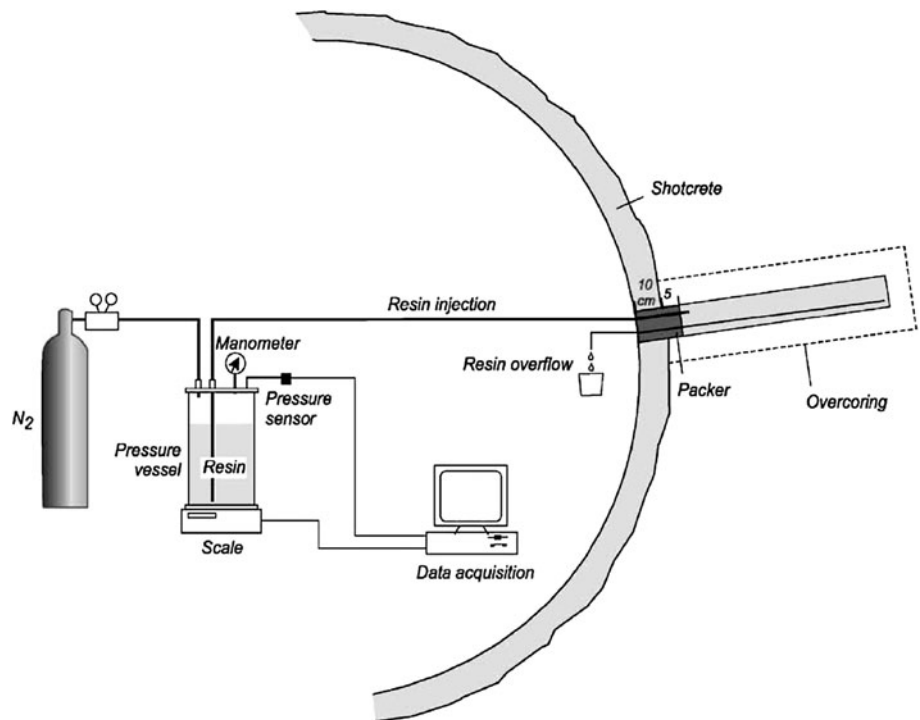


Fig. 5 Experimental design of resin injection. The injection-boreholes for this project are either vertically or horizontally oriented (after Bossart et al. 2002)



second packer is generally placed as close as possible to the rock surface. However, the sealing length of the mechanical packers is 150 mm and often the shallowest part of the rock mass is too fractured for placing a packer. The second

injection is identical to the first one, except that several resin charges are necessary since fracturing is much higher close to the tunnel wall. In this case also, the pressure within the interval is maintained during the whole injection

test. After about 1 h, the polymerization (exothermic heat production and increase of viscosity) makes it necessary to stop the injection.

The properties of the resin used guarantee an ideal impregnation of the open fractures (Table 2). Based on earlier laboratory studies, the requirements for successful fracture impregnation are a low viscosity resin at rock temperatures, density close to that of water, fairly long polymerization time greater than 1 h and a tensile strength of at least 5 MPa. A long polymerization is necessary for completely filling the fracture network and the tensile strength must be high enough to resist the subsequent overcoring process. Furthermore, the resin used retains its volume during polymerization without any shrinking or swelling and the process is not highly exothermic.

3.3 Permeability Measurements

3.3.1 Equipment

Low-permeability clay formation requires a long time to return to its original pore pressure after any disturbance. Hydraulic pore pressure and permeability measurement at this formation requires equipment with long-term stability, resistant to high pressure and allowing the fastest possible return in pressure. Often these measurements need to be started at the drift construction phase and continued for longer period. This stresses that the equipment must be simple, robust and reliable.

For this, Mini-Multi-Packer-System (designed by Solexperts AG, Fierz et al. 2007) has been selected to define up to six test intervals optimally spread along the borehole. The test interval lengths range 10–20 cm and are isolated by hydraulically inflated packers. The volume of the chamber is reduced in order to ensure rapid buildup and stabilization pressure. The rigid packers limit the

compressibility of the system (Fig. 7). Two stainless steel lines allow continuous monitoring of pressure and the running of pneumatic or hydraulic tests dependent on the saturation degree in the interval. In the following sections of the paper, mainly hydraulic test results are discussed.

3.3.2 Test Procedure

In order to investigate the hydraulic properties of the rock around the opening, several test campaigns have been carried out in dedicated boreholes filled with synthetic water having the Callovo-Oxfordian formation fluid composition to prevent clay degradation as well as osmotic fluxes. The evolution of the permeability into the EDZ over time is not discussed in this paper.

Hydraulic permeability measurements were carried out using pulse test (instantaneous increase or decrease of the pressure) or constant head/rate injection test. Pulse tests were carried out for the intact formation at distance greater than one diameter of the drift's wall. Whereas the intervals situated near to the drift wall were tested with a combination of pulse and constant head/rate injection test. This allowed for better estimation of the hydraulic properties and decreases the uncertainty of the estimates by cross validating the test results. The pressure differences imposed on the tests were kept low (<5 bars) to prevent the formation of new fractures.

The tests have been interpreted with the software MULTISIM (Tauzin and Johns 1997), a flexible borehole simulator for the analysis of single phase hydraulic tests in low-permeability formations.

This simulator can account for the following situations:

- Liquid or gas flow.
- Non-ideal test conditions due to variable wellbore storage, wellbore temperature variations and pre-test pressures.

Fig. 6 Strategy for resin injection at long sub-horizontal boreholes of 4.5 m length and a diameter of 42 mm, slightly inclined (swisstopo)

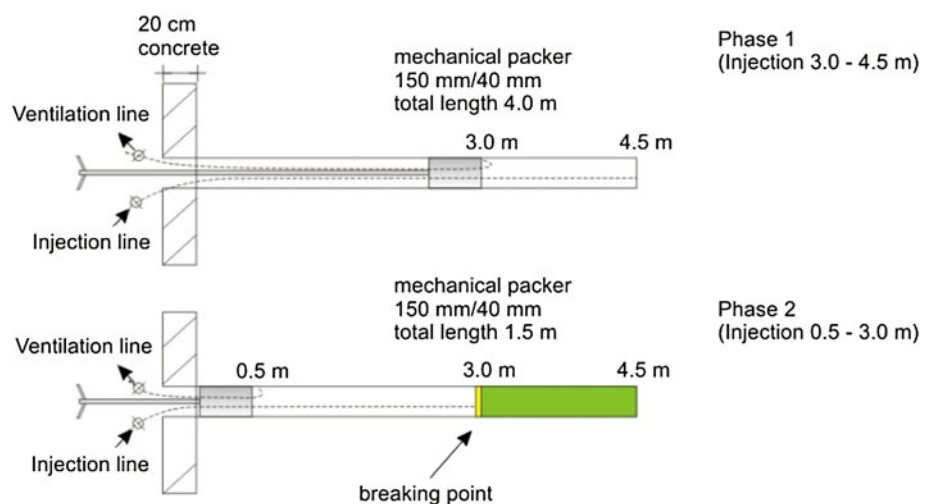
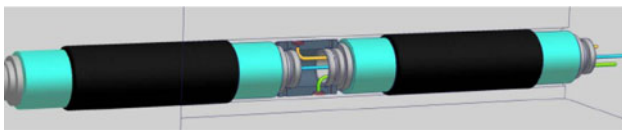


Table 2 Selected chemical and physical properties of the epoxy resin SIKA injection26 (resin manufactured by SIKA AG, Switzerland)

Properties values	
Chemistry	
Epoxy resin free of volatile organic compounds (VOC)	
Resin: bisphenol A/F epoxy resin, modified with reactive and non-reactive extenders	
Hardener: modified, based on aliphatic and cyclo-aliphatic diamines	
Mixing ratio: resin/hardener = 100:51	
Resin is mixable with fluorescene	
Density	
Resin	1.142 (g/cm ³)
Hardener	0.987 (g/cm ³)
Viscosity (development after resin has been injected)	
After 10 min	83 (mPa s) (at 13 °C)
After 30 min	173 (mPa s) (at 13 °C)
After 60 min	452 (mPa s) (at 13 °C)
After 70 min	781 (mPa s) (at 13 °C)
Tensile strength (development after resin has been injected)	
After 3 days	– 2.0 MPa (at 23 °C)
After 7 days	– 7.5 MPa (at 23 °C)
After 14 days	2.0 MPa (at 23 °C) 12.9 MPa (at 23 °C)
After 21 days	4.9 MPa (at 23 °C)
After 28 days	14.6 MPa (at 23 °C)

**Fig. 7** Mini multi packer system: test chamber (Fierz et al. 2007)

- Single and dual porosity, homogeneous or composite formations, fractional dimension flow, no-flow or constant pressure boundaries.
- Any sequence of slug tests, pulse tests, constant pressure tests, constant or variable rate tests.

The general model theory and application for hydraulic permeability test was described by Bourdarot (1996) and Horne (1997). Pickens et al. (1987) provided an application of the method for a radial composite flow, noting that the model assumes a continuous porous medium. ANDRA defined a strategy for the interpretation of hydraulic tests described in Baechler et al. (2011). All tests are interpreted with a radial composite model. The inner zone corresponds to the borehole damaged zone. The discontinuity between inner and outer zones is constrained to a maximal distance of 0.1 m. Moreover, specific storage values are bounded between 10^{-6} 1/m for saturated Callovo-Oxfordian clay and a maximal value of 7.1×10^{-3} 1/m under entirely unsaturated conditions. As the EDZ is a highly complex

and heterogeneous system of fractures/fissures and matrix, the model only allows estimating the average permeability and storage of the formation in the vicinity of the borehole.

As a result, the properties returned by the simulations are representative of a local continuous porous medium around the test interval. Those local properties could not be considered equivalent to the EDZ hydraulic property needed for safety assessment calculation.

4 Characterisation of the Excavation-Induced Fractures Network for Drifts Parallel to the Horizontal Major Stress

4.1 Structural Analysis

4.1.1 Drifts Structural Analysis

Forty-two 3D scan surveys were performed and around 1,200 fractures measured on drifts excavated along the regional major stress axis. Two major structures have been observed on the faces and the walls of the drifts: “chevron” and “bulge” (Fig. 3).

Two types of fractures compose the “chevron” structure. They have the same strike, perpendicular to the axis of the drift, but an opposite dip. These fractures have been generated by normal shear.

On one hand, “lower chevron fractures” (FCh inf.) are localized in the lower third of drift faces and walls. In horizontal plan, these fractures are curved. In the middle of faces, the strike of fractures is perpendicular to drift axis. On the borders of drift’s faces and walls, the strike is oblique, oriented toward the “unexcavated” zone. The dip is oriented toward the excavated zone.

On the other hand, “Upper chevron fractures” (FCh sup.) are localized in the upper part of drift faces and walls. They have the same curve in horizontal plane, but their dip is oriented toward the unexcavated zone.

The “bulge” set of fractures is localized in the middle of faces and walls, between the “upper chevron fractures” and the “lower chevron fractures”. These bulge fractures have been generated by extension. They are plans with a double curve: a bulge form vertically and the same curve as “chevron” fractures horizontally.

4.1.2 Cored Drillings Structural Analysis

Around 4,000 excavation-induced fractures have been analyzed from 400 boreholes. The most significant information about induced fractures was obtained from drilling performed on the walls of the drifts parallel to major stress. In GET drift, 12 horizontal boreholes were performed in a narrow space. Optical imaging of these boreholes was

carried out systematically to identify the dip and orientation of the fracture plan. Based on the data obtained, a 3D representation of the fracture plan in the GET drift was prepared (Fig. 8). Two different zones of excavation-induced fracturing can be clearly distinguished. The first zone near the drift consists of traction and shear fractures. The orientation of both types of fractures is very heterogeneous with high dip fractures. The second zone, farther from the drift consists of shear fractures only. Their orientation is more homogeneous with low dip fractures. In the homogeneous orientation zone, we can extrapolate fractures and associate them to the fractures observed in drifts. The strike of these fractures is nearly parallel to drift axis (0–10°). Fractures can be classified into two major families (Fig. 10a). In the drift’s upper part, fractures have a dip oriented to the block. They correspond to the extension of “upper chevron fractures” in the block. In the drift’s lower part, fractures have a dip oriented to the drift. They correspond to the extension of “lower chevron fractures” in the block. At the middle of the height of the drift, these structures join or intersect each other. Figure 9b shows the extrapolation of the observed fractures to determine a model of the fractures network.

The extent of excavation-induced fractures was determined taking into account all the information and boreholes data in different directions. The analysis distinguishes the extent of extensional fractures and the shear fractures. Table 3 shows the lateral extension of induced fracture zone in two drifts parallel to the major horizontal stress of the underground laboratory (GCS and GET). These two drifts were excavated with a road header technique but the support is rock bolts type, shotcrete and sliding steel arches in GET and rock bolts and shotcrete

with compressive wedge (cf. 2.3) in GCS. Table 3 provides also the minimum, maximum and average extent measured in field. The extent of two zones shows an important variability: the extent of induced fractures zone is not constant along the drift. Those differences seem to be linked with the span of excavation (1–1.2 m in those cases) but no correlation was found due to the limited number of boreholes and the low frequency of drilling in the axis direction compared to the excavation span. No clear difference was observed between the two drifts GCS and GET. The additional results from GAT excavated with a pneumatic hammer confirm that there is no significant change in the extent of induced fractures with the excavation methods.

Naked eye observation of vertical boreholes does not show fractures induced by drift excavation. But in some boreholes near the wall, cores were broken in cuttings. The presence of cuttings is a mark of damaged rock, probably due to drift excavation or boring. The type of fracture is not defined. The extent is mostly lower than 0.50 m ($0.1 \times D$) and reaches a maximum of $0.15 \times D$.

Figure 10 shows density histograms of the measured excavation-induced fractures, observed from horizontal boreholes in GCS drift. Fracture density is an average number of fractures observed from 20 cm of core. These fractures have been measured from core samples obtained from GCS drift. A total of 445 excavation-induced fractures were measured, 343 of which were shear fractures (77 %) and 102 were traction fractures (23 %). Most of these fractures were generated by shearing. The average density is almost 6.5 fractures per meter in the sidewall of the GCS drift. This density is not homogeneous along the borehole. The number of fractures is greater between 0.30

Fig. 8 3D visualisation of the fractures network in GET drift (CDZ boreholes)

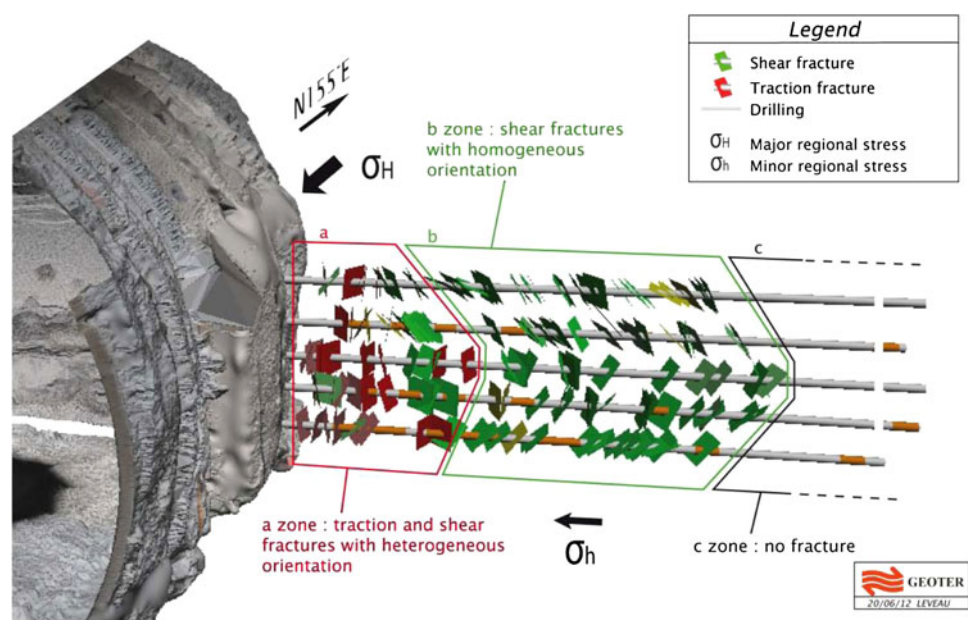


Fig. 9 Setup and orientation of the induced fractures: **a** zoom on the homogeneous zone, **b** proposed conceptual model

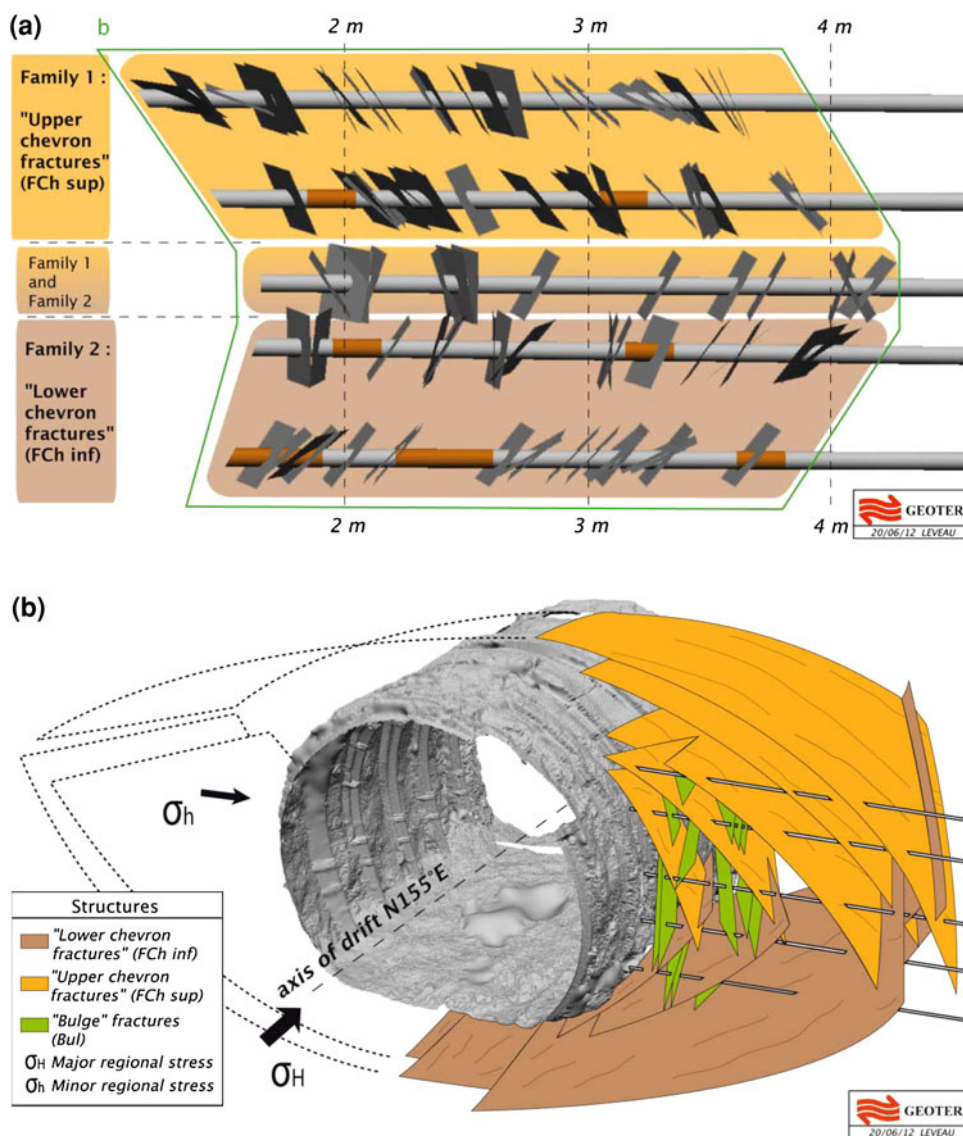


Table 3 Lateral extent of fracture zones at GCS (average diameter 5.34 m) and GET (average diameter 5.44 m) drifts walls (drifts parallel to σ_H)

	Shear fractures extent			Extensional fractures extent		
	Min	Average	Max	Min	Average	Max
GCS						
Meter	3.79	4.45	5.1	0.07	0.96	1.67
Diameter ratio	0.71	0.83	0.96	0.01	0.18	0.31
GET						
Meter	3.85	4.18	4.54	0.38	0.96	1.94
Diameter ratio	0.71	0.77	0.83	0.07	0.18	0.36

and 1.80 m and 3.20–4.60 m from the wall of the drift showing that the density is not decreasing with the length from the wall. Rock is less fractured between 2 and 3 m. It

corresponds to the disappearance of extensional fractures and the decrease of the number of shear fractures. In this zone, some core samples do not have any fracture over 1 m. This zone is the transition between high dip fractures and low dip fractures. Note that the first 20–40 cm of core, in some boreholes, consists of cuttings from drilling. In these cuttings, some fragments showed indication of shear or extensional fractures. However, these fractures were difficult to identify and their orientation could not be estimated. That is why no cuttings data were used to calculate fracture density nor incorporated in the global induced fracture model.

4.1.3 Results from Resin Injection Campaigns

The detailed analysis of a core from sub-horizontal borehole CDZ1331 perpendicular to the wall of gallery GET

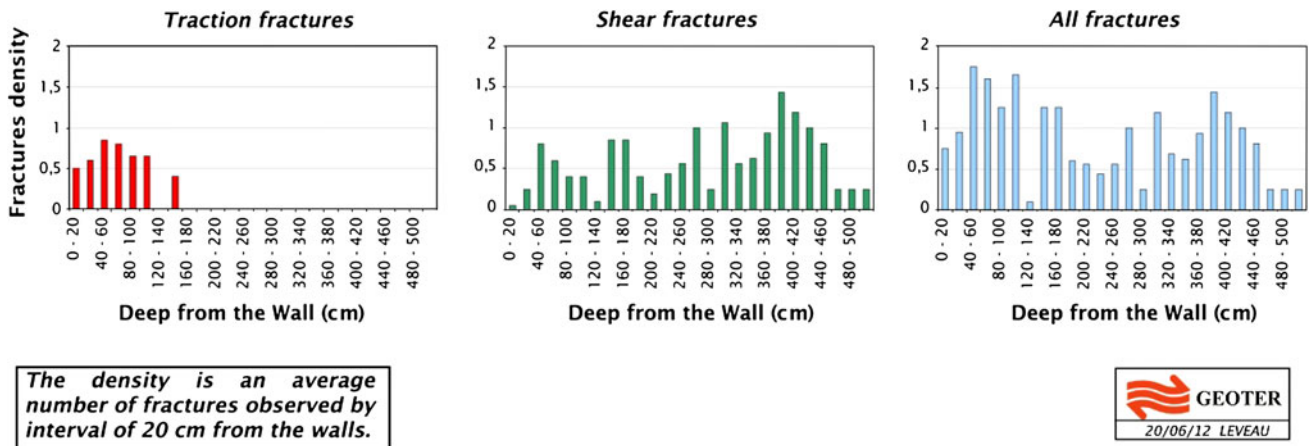


Fig. 10 Fracture density in the GCS drift

Fig. 11 Most important types of excavation-induced fractures found on the CDZ1331 core material

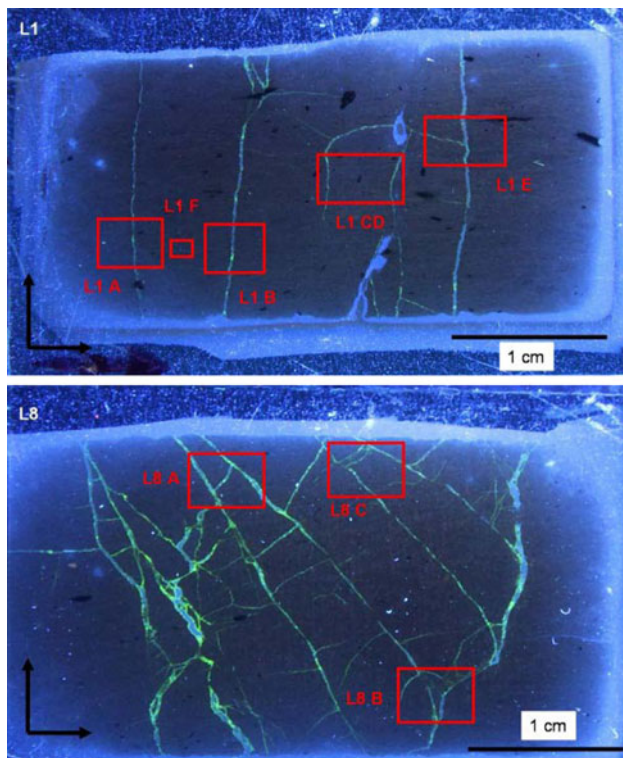
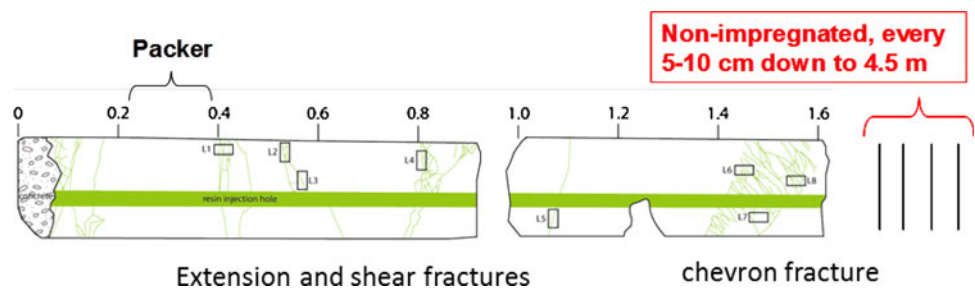


Fig. 12 View of thin sections L1 (onion skin zone) and L8 (shear zone) of borehole CDZ1331 with locations of produced photomicrographs

provides a good example of results obtained with the resin injection method.

Based on the resin impregnated fracture analysis, the core can be divided into three main parts (Fig. 11):

- First 1.1 m section behind the gallery wall: the fracture network consists of sub-vertical extensional fractures oriented oblique to the drift axis (Fig. 12, L1) which are identical to the “bulge” fractures at the front face. These fractures developed during the excavation and are strongly controlled by the direction of excavation and the distance to the drift/gallery front (“onion skin”) thus they are mimicking former tunnel fronts during excavation. The fracture network in this zone is heterogeneous.
- Second section between 1.4 and 1.6 m from the gallery wall: a 10-cm thick fracture network zone with an envelope dipping toward the tunnel front with a 60° angle and a strike parallel to the tunnel axis (Figs. 12, L8 and 13). According to its strike and dip, this shear zone may correspond to the lower part of a shear chevron fracture.
- Third section between 1.9 and 4.5 m from the drift/gallery wall: a rather homogeneous network of non-impregnated shear fractures dipping 83° toward the gallery is present. The fractures occur every 5–10 cm and are oriented parallel to the tunnel axis.

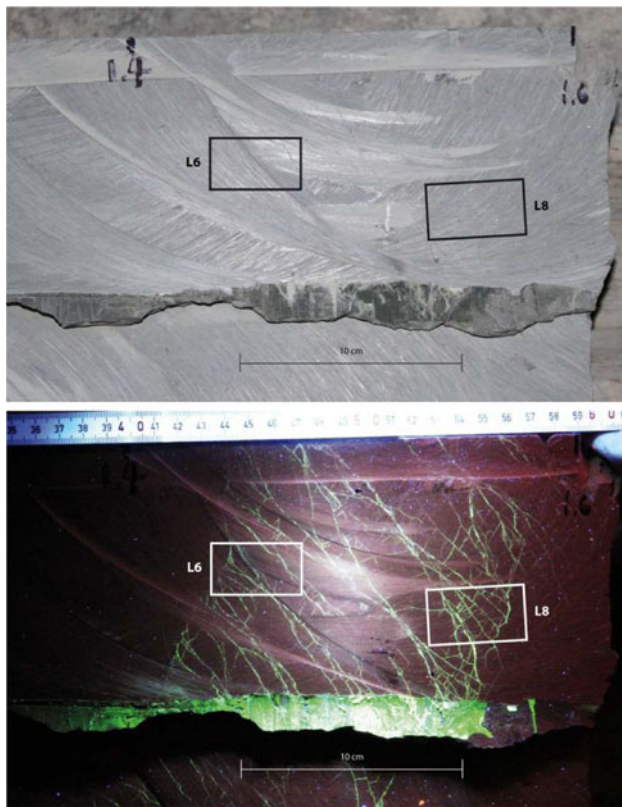


Fig. 13 Plane light (*top view*) and UV-light (*bottom view*) of the core section between 1.4 and 1.6 m of borehole CDZ1331. The complex fracture network is only visible under UV light. Thin section L8 is displayed in Fig. 13

Despite the effort to perform the resin injection in two steps at 0.2 and 3.0 m, no impregnated fractures were identified deeper than 1.6 m from the gallery face. Even the thin sections did not reveal any traces of fractures. However, non-impregnated shear fractures are present up to 4.5 m from the gallery wall/face. The most reasonable explanation on the extent of non-impregnated fractures is the tensile and shearing nature of fractures within the first 1.6 m section behind the tunnel wall which results in a larger aperture and consequently no resin impregnation. Within the homogeneous zone larger than 1.9 m, shear fractures are not impregnated despite a 12 bars injection pressure. This means that shear fractures are nearly closed. Concerning the geometry and frequency of the induced fractures around a tunnel, the results of resin injection method are consistent with the result of traditional geological survey.

Four boreholes OHZ1761–OHZ1764 have been used to get a complete radial profile/section, providing new insights into the induced fracture structure around the GCS gallery. The results confirm the previous observations of GET and structural analysis in drift parallel to the major horizontal stress. The deepest resin impregnation fractures

could be found at 1.9 m behind the tunnel wall. At the two sub-horizontal boreholes down to 1.1 m behind the tunnel wall, the fracture network consists of sub-vertical extensional fractures with orientations oblique to the tunnel axis. Behind this zone, fractures are typically not impregnated with resin and oriented parallel to the tunnel wall (dipping 80–90° toward the gallery), which corresponds to the homogeneous zone with fractures of a shear origin only, according to the results from the structural analysis.

A discrepancy with the structural analysis is noticed for the vertical boreholes. The deepest resin impregnated fractures is found at 1.7 m at the roof, which is nearly twice deeper than the last fracture observed on cores. The two vertical boreholes show a dense pattern of densely spaced fractures uniformly oriented sub-parallel to the axis of the tunnel. A distinction between a shallower heterogeneous and a deeper homogeneous zone cannot be made there. Not all fractures are going through the core, which can explain why they could not be seen by naked eyes, but most fractures are crossing the core and were seen by structural analysis. In fact, nearly no sub-parallel fractures have been identified on vertical cored boreholes farther than 0.7 m in more than 20 boreholes. Then the question arises whether the resin pressure injection was too high and able to open bedding plans in those areas where the rock is already damaged by the excavation.

For the statistical analysis of the observed resin impregnated fractures, a scan-line was placed 6 cm below the top of the core half. Apertures along the scan-line were measured perpendicular to the cracks and not parallel to the scan-line, so real apertures were measured. In CDZ1331, the shallow part of the borehole, apertures of up to 0.8 mm have been measured. The fracture zone near 0.8 m is mainly dominated by a single large fracture with almost 0.7 mm aperture and the rest of the fractures range between 0.1 and 0.4 mm. The shear zone exhibits fractures of apertures between 0.1 and 0.7 mm. It is important to note that with a scan-line parallel to the borehole axis in this specific case, interconnecting sub-horizontal fractures are systematically not recorded because they are not intercepted by the line. Note also that the largest (>1 mm) and the smallest fractures (<100 μm) are not recorded with this method.

The frequency of fractures as a function of depth reveals that the highest frequency is found at about 0.8 m (13 fractures per 10 cm) and also between 1.4 and 1.6 m in the chevron zone (19 fractures per 10 cm). In the shear zone, more fractures are present than in the whole shallower part of the borehole. Note that the packer was located between 0.2 and 0.4 m and thus data shallower than 0.4 m might not be representative.

Two separate scan-lines have been measured focusing on the core. Profile (a) was placed about 10 cm from the

top of the core and profile (b) about 4 cm from the top, both parallel to the borehole axis (Fig. 14a). The plot of frequency of fractures versus aperture (Fig. 14b) shows a comparable lognormal distribution for both scan-lines with highest frequencies for apertures of 0.2–0.4 mm. The plots in between frequency of fractures versus depth along the two scan-lines are very comparable (Fig. 14). The two datasets yield both a bimodal distribution crossing the shear zone parallel to the borehole axis. The shift of about 2.5 cm between the two distributions is a geometrical artefact due to the dip of the fracture zone. Cumulative fracture aperture along a borehole can be an important insight to analyse drift convergence.

4.2 Model of Excavation-Induced Fractures Network Around Drifts Excavated Parallel to the Major Horizontal Stress

Based on the results of drifts and boreholes geological survey, and on resin impregnation data, a model of excavation-induced fractures network around the drifts parallel to major horizontal stress is proposed in Fig. 15. Shear fractures are more widespread and expand deeper in the rock. Extensional fractures are located near the wall with a more heterogeneous dip and strike. This model tries to represent the strike and dip of different types of fracture in different cross sections. The heterogeneity of the network is not properly represented in the model due to the variability of its extent variation along the digging axis. This heterogeneity (in term of extension and density) is not correctly explained. One can assume than this variability of its extent may be related to the step of excavation, but the frequency of boreholes along the digging axis is not sufficient to conclude on this correlation. But the general understanding of the geometry of the fracture network is considered in the model.

Figure 16 shows the front of a drift excavated perpendicular to a drift parallel to σ_H , at 3.5 m from the wall. The footprint of the chevron fracture is well identified and confirms the reliability of the proposed model. Note that the shape of the excavated fracture network around openings parallel to σ_H seems to be similar even at a smaller scale for 5 cm diameter boreholes and 0.7 m diameter micro-tunnel (Fig. 17). All excavations (drifts, boreholes, micro-tunnel) exhibit roughly identical excavation-induced fractures network (type of fractures, geometry, extent). The lateral extent of the shear fractures zone for smaller opening is almost equal to 1 diameter of the opening, suggesting that there is no significant scale effect from a borehole of 5 cm diameter to a drift of 5 m diameter.

4.3 Hydraulic Conductivity Measurements

In a fractured claystone, interpretation of hydro-geological tests is difficult due to the unsaturated condition of the rock and the variability of the hydraulic conductivity. It has been shown on fracture in laboratory (Davy et al. 2007) and in situ (Meier et al. 2001) tests that when the fracture or the fractures network are saturated with water (in chemical equilibrium with the medium), hydraulic conductivity decreases with time. This decrease of fracture transmissivity is due to the strong interactions between interstitial water and argillite minerals. To compare the saturated hydraulic conductivity determined at different times, test intervals were first fully saturated under constant head injection and tested in saturated condition under which the swelling effect was observed. The same procedure was followed in all test intervals of boreholes to allow comparison in between different intervals. In this paper hydraulic conductivity change as function of time is not discussed.

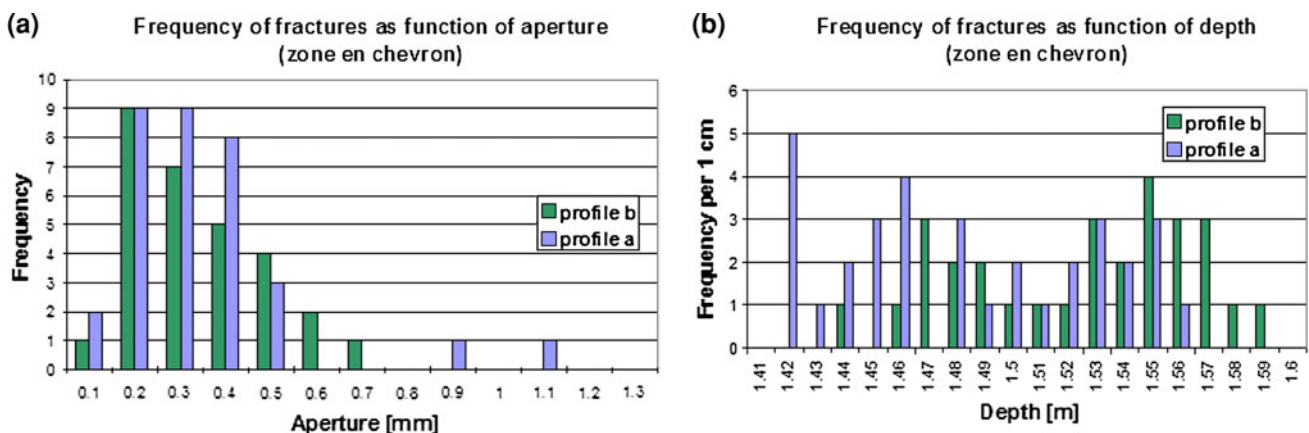


Fig. 14 Frequency of resin impregnated EDZ fractures along two profiles crossing the zone en-chevron between 1.4 and 1.6 m **a** as function of aperture. **b** As function of depth (m)

Fig. 15 Conceptual model of the induced fractures network around a drift parallel to the horizontal major stress

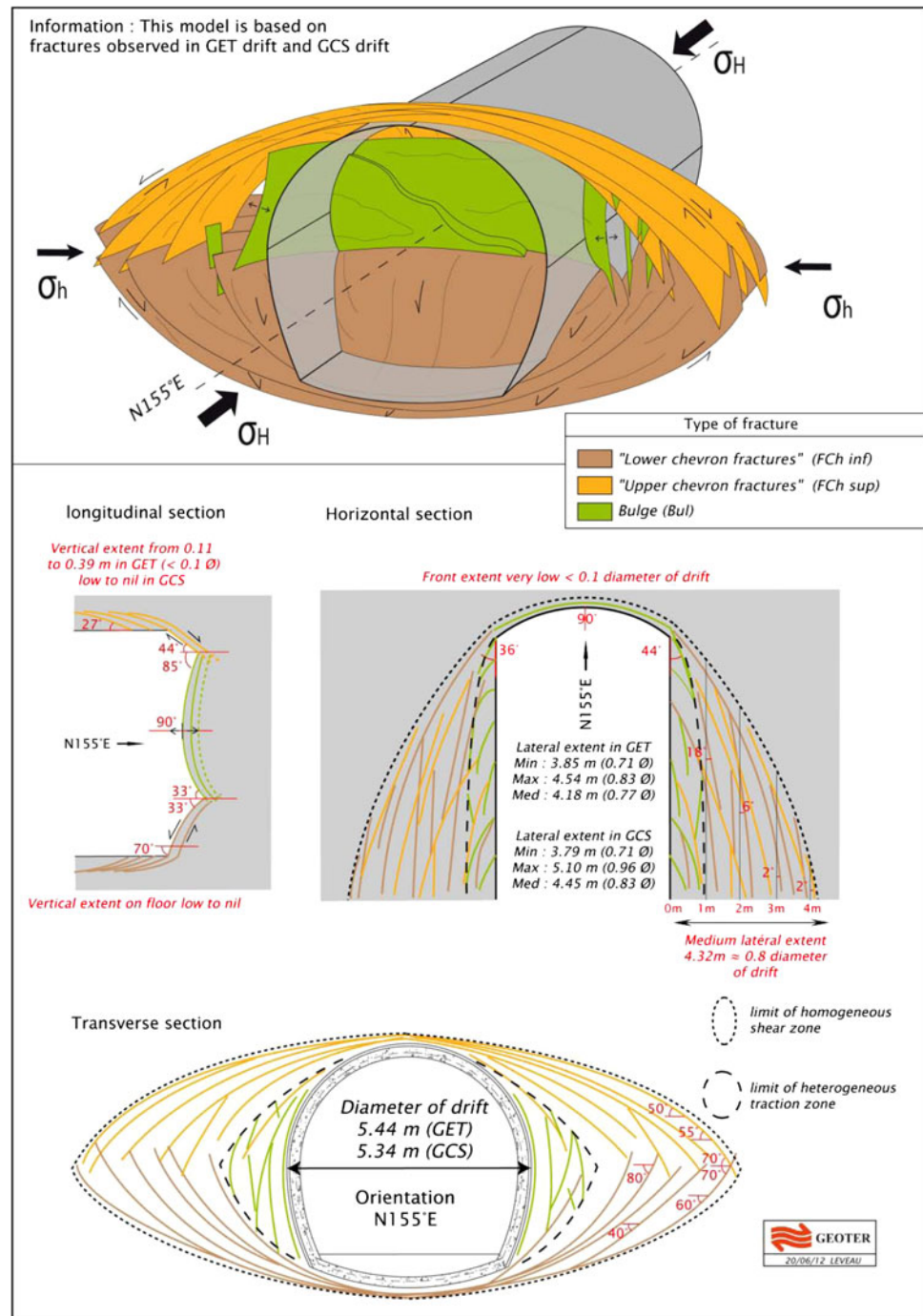
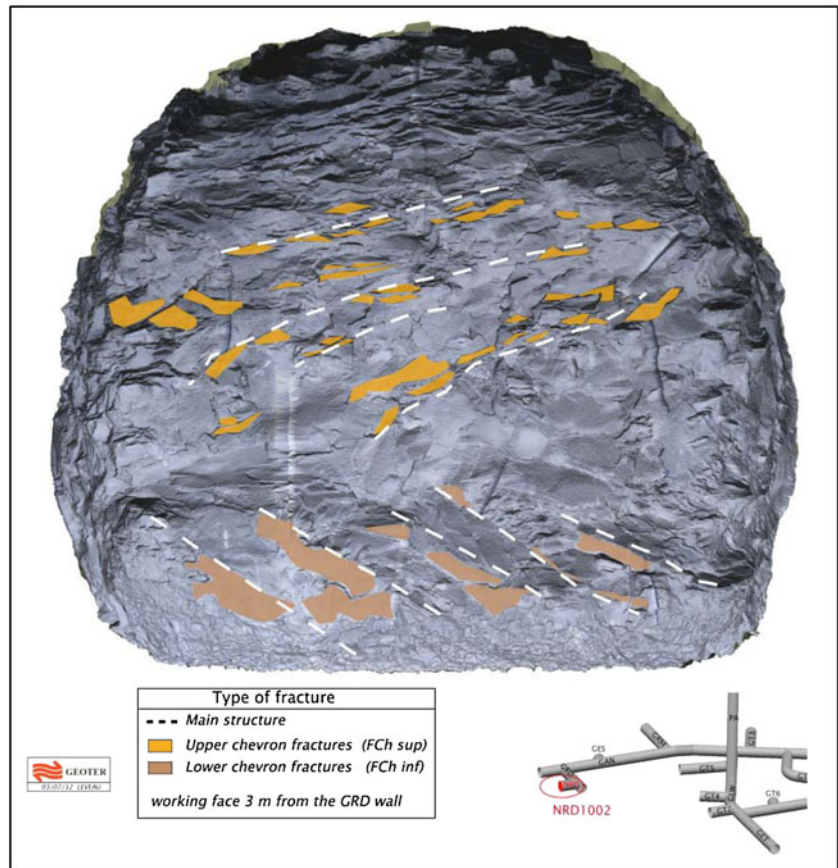


Figure 18 presents the values of hydraulic conductivity in eight boreholes, drilled 6 m from drift GCS (parallel to the major horizontal stress). Sensitivity analysis has shown that the uncertainty in hydraulic conductivity measurements is between half and one order of magnitude. The highest hydraulic conductivity is observed in test intervals where fractures cross the borehole. The estimated permeability from the test analysis is not representative of the hydraulic properties of the continuous rock matrix, but of the fractures transmissivity. This is confirmed by the

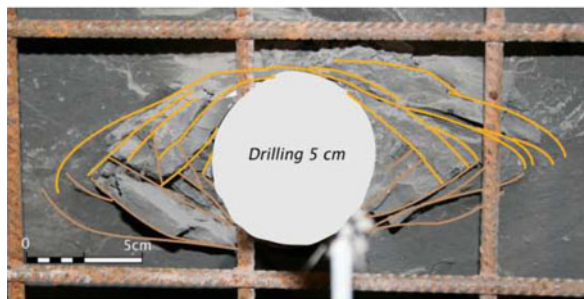
hydraulic tests performed on core rock samples collected between fractures indicating hydraulic conductivity lower than 1×10^{-12} m/s.

In Figure 18, the extent of extensional fractures and purely shear fractures is also plotted for each borehole. In all boreholes, the conductivity generally diminishes with increasing depth from the excavation wall. The highest conductivity is found in the extensional fractures zone. For horizontal boreholes at the wall (Fig. 18a), the highest conductivity is higher than 10^{-9} m/s and is located

Fig. 16 View of the front of a drift at the intersection with drift parallel to σ_H : shear chevron fractures



(a) Fracturation induced by N155°E drilling (regional major stress axis)



(b) Fracturation induced by N155°E micro-tunnel (regional major stress axis)

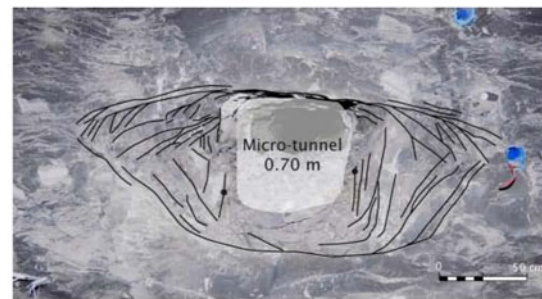


Fig. 17 Induced fracture network around opening parallel to σ_H : **a** around a borehole of 5 cm diameter. **b** Around a micro-tunnel of 0.7 m diameter

at <0.5 m from the wall. In the extensional fractures zone, hydraulic conductivity varies from 1.7×10^{-9} to 4×10^{-12} m/s. In the area with only shear fractures, an overall slight decrease of conductivity is observed from 6×10^{-12} to 1×10^{-12} m/s. In some boreholes, like OHZ1731 and OHZ1735 in area of only shear fractures, the conductivity does not decrease regularly with increasing depth from the wall. This can be due to the fact that in this

zone, some chambers cross fractures entirely or partially while others do not. Considering the uncertainty on the hydraulic conductivity analysis, it could be considered that the hydraulic conductivity is nearly equal to the conductivity of the undisturbed rock beyond a distance of one diameter from a drift or a borehole.

For vertical boreholes at the floor and roof (Fig. 18b), the hydraulic conductivity varies from 8×10^{-8} to

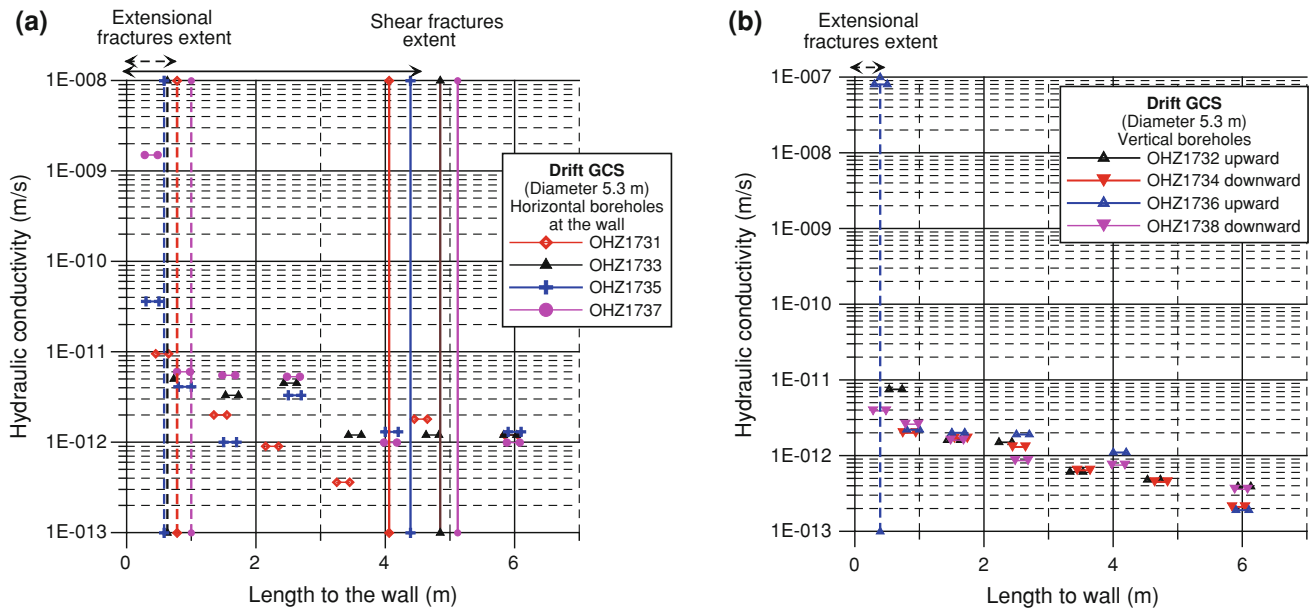


Fig. 18 Hydraulic conductivity measured in drift GCS (parallel to σ_H): **a** horizontal borehole at the wall, **b** vertical boreholes at floor and ceiling

5×10^{-12} m/s in the extensional fractures zone. It can be noticed that extensional and shear fractures were observed only in borehole OHZ1736, while no induced fracture crossed the other boreholes. Even without any induced fractures, a slight decrease of conductivity is observed from 7×10^{-12} to 2×10^{-13} m/s from 0.5 to 6 m to the wall. At one radius from the wall, conductivity measured in chambers is of the same order of magnitude as the undisturbed claystone at the main level of the URL.

5 Characterisation of the Excavation-Induced Fractures Network for Drift Parallel to the Horizontal Minor Stress

The same type of analysis has been performed around GED drift parallel to the horizontal minor stress.

5.1 Induced Fractures Network Model

The same types of fractures were identified in walls, fronts and cores around drifts parallel to σ_h as for σ_H , but their geometry (strike, dip and extent) is different:

1. The shear chevron fractures are initiated ahead of the excavation face during excavation. They form symmetrically to the horizontal plane crossing the gallery axis. The fracture dip is around 45° . Extension of the chevron zone ahead of the excavation face is between 0.5 and 1 drift diameter (about 4 m). The shear

fractures were not impregnated with resin at the ceiling and roof.

2. Shear vertical and oblique fractures formed beyond the chevron fractures end at them. These fractures are oriented at a low angle ($10\text{--}30^\circ$) with respect to the wall. This fracture system was identified only in drill cores from the sidewall. It shows sub-horizontal lineation (strike slip kinematics). The shear fractures were not impregnated with resin because they were closed in in situ condition.
3. Unloading tensile fractures: This fracture system is identified all around the drift (sidewall, vault and floor). Most fractures are parallel to the drift wall, partially connected together by shear splays. This fracture system is comparable to the onion skin fracture identified at Mont Terri URL (Bossart et al. 2002), but is very limited in number (1–2) and limited to a maximum depth of 0.5–0.7 m, whatever the direction considered. Most fractures initiated in extension mode were impregnated with resin.

Figure 19 presents the proposed model of excavation-induced fractures for drift parallel to σ_h . It can be noticed that most of the fractures represented in the 3D view are shear fractures, because they extend more than extensional fractures. Near the wall, the dip and strike of both types of fractures are nearby and are difficult to distinguish in a 3D view. Table 4 gives the extent of the extensional and the shear fractures. The description of this network is not as significant because less data are available especially at

Fig. 19 Conceptual model of the induced fractures network around a drift parallel to the horizontal major stress

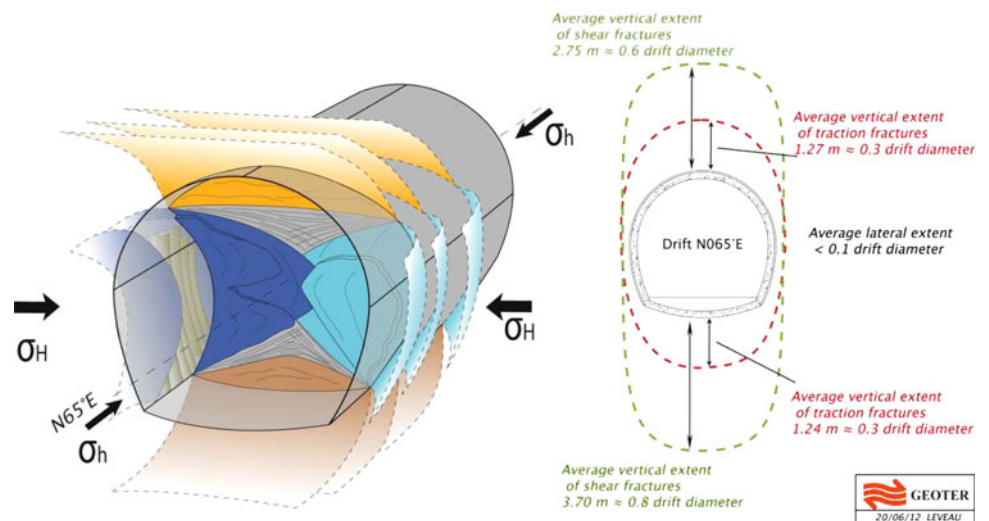


Table 4 Extent of fractures zone (ratio of drift diameter from the wall) for a drift parallel to σ_h

	Extensional fractures extent			Shear fractures extent		
	Min	Average	Max	Min	Average	Max
Ceiling	$0.2 \times D$	$0.3 \times D$	$0.4 \times D$	$0.5 \times D$	$0.6 \times D$	$0.8 \times D$
Wall	$0.1 \times D$	$0.1 \times D$	$0.2 \times D$	–	–	–
Floor	$0.2 \times D$	$0.4 \times D$	$0.5 \times D$	$0.8 \times D$	$0.8 \times D$	$1.1 \times D$

‘–’ no extent farther the extensional fractures network

$\pm 45^\circ$. Further investigations are planned in drift parallel to σ_h to confirm the model.

5.2 Hydraulic Conductivity Measurements

Hydraulic conductivity was measured in the horizontal and vertical boreholes drilled at the wall of the GED drift (Fig. 20). The pneumatic test alone was carried out in the first chamber of SDZ1242 and SDZ1243 at 0.6 m depth. The discrepancy between the results of pneumatic and hydraulic test is related to the rock self-sealing process which reduces the hydraulic conductivity. It was noticed that the hydraulic conductivity in GED drift is slightly lower than that in the older GMR drift (Armand et al. 2009).

Hydraulic tests carried out in horizontal boreholes estimated the hydraulic conductivity to be lower than 10^{-10} m/s even in the fracture zone. On the side wall unloading and shear fractures are not widespread and test intervals do not always cross fracture. This can explain that hydraulic conductivity remains low at some location. At less than a radius from the wall, hydraulic conductivities were comparable to that of the undisturbed rock. For vertical boreholes, hydraulic conductivity higher than 10^{-10} m/s was observed in the first 2 m from the drift which is included in the area of extensional fracture. Deeper into the rock, hydraulic conductivity decreases as a function of depth and at one diameter from the wall it approaches the value of

undamaged rock. In the shear fracture zone, transmissivity of the shear fracture seems to have a low impact on the hydraulic conductivity. It was confirmed by the fact that pore pressure reached 1 MPa in the chamber between 4 and 5 m from the wall.

Generally, measurements in drifts parallel to σ_h exhibit the same behavior than in drifts parallel to σ_H , but not at the same location:

1. Highest hydraulic conductivity was observed only in the area where extensional fractures were located.
2. Deeper into the rock, hydraulic conductivity decreases from 10^{-10} to 10^{-12} m/s within a few meters.
3. The location of high hydraulic conductivity differs because induced fractures network depends on the drift orientation in relation to the in situ state of stress.

6 Discussion

6.1 Induced Fractures Network Formation

Initiation and propagation of micro-cracks may lead to mechanical damage of Callovo-Oxfordian claystone material, which may finally result into failure/collapse by the coalescence of micro-cracks into organized fractures. During tunnel/drifts construction new surfaces are created thereby generating significant changes in the local stress

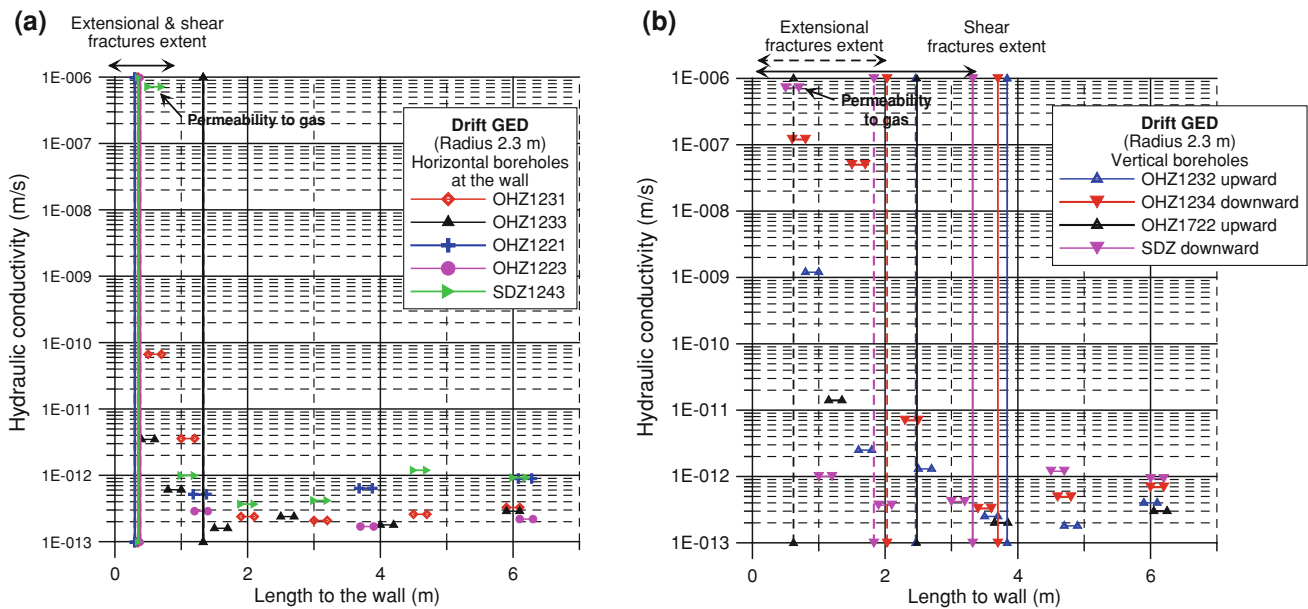


Fig. 20 Hydraulic conductivity measured in drift GED (parallel to σ_h): **a** horizontal borehole at the wall, **b** vertical boreholes at floor and ceiling

field. Near the wall, the confining stress becomes zero and the other stress components increase, which may lead to local failure under extension and/or shear. Taking such stress paths into account, the failure behaviour can be quite different for different rock types under different in situ stress states. Blümling et al. (2007) described well the type of failure that can be observed in a claystone by assuming that the failure behavior that Diederichs (2003) suggested for crystalline rocks can be generalized. They explain that more competent rock like hard clays or clay shale tend to show spalling or extensional failure as the spalling conditions are reached first, while soft rocks may preferentially fail under shear. In the case of anisotropic rocks, an activation of the planes of weakness can also be observed.

The structural data presented in the previous sections provide a comprehensive description of the organization of the induced fracture network at the main level of the URL. That clearly shows that the first and paramount failure mechanism is shear which occurs from the front. Extensional failure due to spalling occurs during the drift convergence and is less developed ($\approx 75\%$ of the total number of fractures are shear fracture). The chevron shape fractures are similar to those observed at Mol as described by Wileveau and Bernier (2008), but no spalling was observed in plastic clay. As opposed to Blümling et al. (2007) statement, in the Callovo-Oxfordian claystone at the main level of the Meuse/Haute-Marne URL, spalling is not the prevailing mechanism of failure, due to the fact that the in situ level of stresses is high. The Opalinus Clay at Mont Terri exhibits similar rock strength and shows distinct extensional failure along the tunnel wall (Bossart et al.

2002). There, the general structure of the EDZ is controlled by extension fracturing, bedding plane slip and geological fault. The thinner overburden at Mont Terri URL results in lower in situ stress compared to the Meuse/Haute-Marne URL, and reduces the occurrence of shear failure. These stress differences along with the presence of a fault and pronounced bedding planes in the Opalinus clay, explain the difference between the excavation-induced fractures conceptual model at the Meuse/Haute-Marne URL with the “onion skin fracture” model proposed by Bossart et al. (2002) at the Mont Terri URL.

6.2 EDZ at the Main Level of the Meuse/Haute-Marne URL

The notion of EDZ is complex in the sense that it is not an intrinsic property of the rock but refers to the notion of safety. Tsang et al. (2005) suggested distinguishing excavation disturbed zone (EdZ) and excavation damaged zone (EDZ) enforceable for all types of rock, stating that:

1. The excavation disturbed zone (EdZ) is a zone where only reversible mechanical and hydrological processes occur without resulting in major changes in flow and transport properties.
2. The excavation damaged zone (EDZ) is a zone with significant irreversible processes and significant changes in flow and transport properties.

In the field it is not easy to determine limits between EDZ and EdZ because the terms “major changes” and “significant change” are not clearly defined.

Lanyon (2011) introduced another concept within the EDZ: the highly damaged zone (HDZ) is defined as a zone where macro-scale fracturing or spalling may occur. The effective permeability of this zone is dominated by the interconnected fracture system and may be orders of magnitude greater than the undisturbed rock mass. As defined, HDZ is doubtlessly part of the EDZ.

So the discussion about EDZ around the drift should be carried out according to Tsang et al. (2005) definition with the performance assessment point of view and also for in situ determination of the significant properties. In 2003 Bauer et al. reported the following conclusions from a preliminary performance assessment performed for the Callovo-Oxfordian claystone (similar to what is observed in the Meuse/Haute-Marne URL).

- Considering permeability of sealing systems lower than, or equal to 10^{-10} m/s, and a damaged zone with a permeability not higher than two orders of magnitude than the undisturbed rock permeability, the geological barrier is the main radionuclide transfer pathway;
- If the seals do not cut off the fractured zone around the openings and if the latter is continuous with permeability higher or equal to 10^{-9} m s⁻¹, EDZ provides a short circuit of the geological barrier.

As a performance assessment assumption, a permeability value of 10^{-9} m s⁻¹ (for a porous equivalent media) can be considered as a limit defining EDZ for the Meuse/Haute-Marne URL.

Another point arises, if significant changes occur in flow and transport properties relevant for performance assessment or remain active in the long term, when the surroundings of drift are fully saturated. In claystone, self-sealing of the fracture network occurs (Bock et al. 2010). This was demonstrated by repetitive hydrotesting carried out over more than 2 years at Mont Terri. During these tests, the fracture transmissivity decreased by almost one order of magnitude per year (Meier et al. 2001). On Callovo-Oxfordian samples, Davy et al. (2007) showed that fissures transmissivity decreases only in a few days and the

permeability approaches the permeability determined in undisturbed claystone. These results were also obtained under in situ condition at the Meuse/Haute-Marne URL. The relevant self-sealing process may be osmotic swelling of the fracture walls, but other processes such as rock-creep are probable. However, these processes still need to be better explained at the micro scale. This emphasizes that an EDZ could be created during excavation work, could be extended before repository closure (due to moisture content for example) and could even disappear (in terms of transport properties) when it is fully saturated.

In this paper, only the initial EDZ occurring after the drift construction is discussed. Evolution of the EDZ over time during drift lifetime and under saturation is a key research program performed at the Meuse/Haute-Marne URL, adapting methods and interpretation of hydraulic/pneumatic tests to follow this evolution over time (Baechler et al. 2011).

The hydraulic conductivity or permeability measurements presented in the previous section indicate that the permeability values in chambers crossing fractures is observed to be less than or equal to 10^{-10} m s⁻¹ with extensional fractures more or less connected to the wall. Taking into account Bauer et al. (2003) and the permeability measurements, a threshold value of permeability equal to 10^{-10} m s⁻¹ could be considered as the upper permeability limit of the EDZ for the Meuse/Haute-Marne URL. By comparing the permeability measurements with the structural analysis, it can be concluded that all chambers in which estimated values of permeability are higher or equal to 10^{-9} m s⁻¹ are crossed by or near fractures located in the zone where extensional fractures have been observed. On the other hand, all the fractures located in the zone with extensional fractures do not necessarily exhibit high transmissivity with average permeability $<10^{-10}$ m s⁻¹. Then, the extent of tensile fracture zone could be considered as an upper bound of the EDZ extension at the main level of the Meuse/Haute-Marne URL. The EDZ is mainly the connected fracture network with shear and extensional fractures. It is also shown that in this claystone, we have to

Table 5 Extent of EDZ and EdZ (ratio of drift diameter from the wall)

Drift orientation	Extensional fractures extent			Shear fractures extent			EDZ extent Max	EdZ extent Max
	Min	Average	Max	Min	Average	Max		
N65//σ_h								
Ceiling	0.2 × D	0.3 × D	0.4 × D	0.5 × D	0.6 × D	0.8 × D	0.4 × D	0.8 × D
Wall	0.1 × D	0.1 × D	0.2 × D	–	–	–	0.2 × D	0.6 × D
Floor	0.2 × D	0.4 × D	0.5 × D	0.8 × D	0.8 × D	1.1 × D	0.5 × D	1.1 × D
N155//σ_H								
Ceiling	–	0.1 × D	0.15 × D	–	–	–	0.15 × D	0.5 × D
Wall	0.01 × D	0.2 × D	0.4 × D	0.7 × D	0.8 × D	1.0 × D	0.4 × D	1.0 × D
Floor	–	0.1 × D	0.15 × D	–	–	–	0.15 × D	0.5 × D

–No extent farther the extensional fractures network

distinguish the mechanical damage and the EDZ, as defined by Tsang et al. (2005). In fact, the propagation of shear fractures is larger than the extent of the EDZ. In our case, the EDZ is exactly what Lanyon (2011) described as HDZ.

Deeper into the rock, the permeability decreases slowly with depth and becomes equal to the permeability of intact rock mass at around a diameter from the excavation wall and that zone defines the EdZ. The EdZ envelope is delineated by the end of the shear fractures. These shear fractures can be observed but they do not affect much the average permeability, like on the side wall of drift parallel to σ_H . Also, micro-crack and/or porosity change which implies slight change in permeability do not affect much the average permeability like at the ceiling of drift parallel to σ_H . Table 5 summarizes the extent of EDZ and EdZ as a function of stress orientation.

7 Conclusions

An important characterization of induced fracture network around openings has been conducted at the main level of Meuse/Haute-Marne URL by structural analysis of the front face and walls, the analysis of cores and resin impregnated cores. Permeability measurements have been carried out with multi-packers systems allowing up to six test intervals optimally spread along the borehole. Drift excavations at the main -490 m level of the URL exhibit extensional and shear fractures that were not observed in drifts at the -445 m level. Spalling is not the prevailing mechanism of failure due to the high level of average stress compared to the Callovo-Oxfordian claystone strength. Shear failure seems to occur first from the excavation front face. Shear band has been observed by the resin impregnation method at smaller scale confirming the shear failure mechanism. The fracture pattern and extent depend on the drift orientation versus the in situ state of stress:

- Drifts parallel to σ_H show, at the most, extensional and shear fractures up to 0.4 diameter and one diameter from the wall. At the roof and ceiling, shear and extensional fracture zones are mixed up to 0.15 diameter.
- Drifts parallel to σ_h show, at the very most, extensional and shear fractures up to 0.5 diameter and one diameter respectively at the roof and the ceiling. At the wall, shear and extensional fracture zones are mixed up to 0.2 diameter.

The area with unloading fractures exhibits the highest hydraulic conductivity locally above 10^{-10} m/s. Those high values are due to the fracture transmissivity and not the permeability of the rock matrix. Farther from the wall,

the shear fractures exhibit low transmissivity which did not affect considerably the average hydraulic conductivity.

Taking into account Tsang et al. (2005) definition of the EDZ and the discussion based on the hydraulic conductivity results, it is shown that the excavation-induced fracture zone extent is larger than the EDZ. The EDZ is included in the zone with extensional fracture in the Callovo-Oxfordian claystone at the Meuse/Haute-Marne URL. In other words, due to the self-sealing processes occurring in a claystone, the mechanical damage (fractures) does not always result in a significant change in hydraulic properties. Structural analysis has been performed on numerous boreholes in the URL to infer the extent of shear and extensional fractures and the EDZ. Beyond the EDZ, EdZ is associated with diffuse damage with no more extensional fractures.

For long-term performance assessment, the initial state of the EDZ will be considered at the time of repository closure, meaning that it is necessary to investigate the effect of ventilation and saturation on the hydraulic properties of the EDZ and the possible extent of the EDZ as a function of time. Following the initial characterization, the hydraulic conductivity around drifts continues to be measured to assess the EDZ change over time. A specific experiment called CDZ (“compression of the EDZ”) focuses on the change of hydraulic conductivity in the excavation-induced fractures zone under saturation and normal loading. To optimize the design of the repository support, different excavation and support techniques are being implemented in phases to study over time their effect on the excavation-induced fracture network and the relationship between the fracture zone, the rock deformation around openings and the support loading.

Acknowledgments We gratefully thank P. Lebon and P. Dubreuil for their review and discussions, and A. Rawat and G. Thalagavadi Hallilingaiah for helping us to correct the English and giving their external points of view.

References

- Armand G, Wileveau Y, Morel J, Cruchaudet M, Rebours H (2007) Excavated Damaged Zone (EDZ) in the Meuse Haute-Marne underground research laboratory. In: Ribeiro e Sousa L Olalla C and Grossmann N (eds.) Proceedings of the 11th congress of the ISRM, Lisbon, 9–13 July 2007, pp 33–36
- Armand G, Nussbaum C, Cruchaudet M, Rebours H (2009) Characterisation of the Excavated Damaged Zone (EDZ) in the Meuse Haute-Marne underground research laboratory. In: Proceedings of the International Conference on Rock Joints and Jointed Rock Masses, 4–9 Jan 2009, Tucson
- Armand G, Noiret A, Cruchaudet M, Conil N (2011) Mine by experiment performed in the Callovo-Oxfordian claystone at the Meuse Haute Marne Underground Research Laboratory (France). ISRM 12th International Congress on Rock Mechanics, 9–13 October 2011, Beijing

- Baechler S, Lavanchy JM, Armand G, Cruchaudet M (2011) Characterisation of the hydraulic properties within the EDZ around drifts at level _490 of the Meuse/Haute-Marne URL: a methodology for consistent interpretation of hydraulic tests. *J Phys Chem Earth*. doi:10.1016/j.pce.2011.10.005
- Bastiaens W, Bernier F, Li XL (2007) SELFRAC: experiments and conclusions on fracturing, self-healing and self-sealing processes in clays. *J Phys Chem Earth* 32:600–615
- Bauer C, Pépin G, Lebon P (2003) EDZ in the performance assessment of the Meuse/Haute-Marne site: conceptual model used and questions addressed to the research. In: Proceedings of the EC Cluster conference on Impact of the EDZ on the performance of radioactive waste geological disposal, Luxembourg, 3–5 Nov 2003. European Commission Report EUR21028EN
- Blümling P, Bernier F, Lebon P, Martin CD (2007) The excavation damaged zone in clay formations time-dependent behavior and influence on performance assessment. *Phys Chem Earth* 32:588–599
- Bock H, Dehandschutter B, Martin D, Mazurek M, de Haller A, Skoczylas F, Davy C (2010) Self-sealing of fractures in argillaceous formations in the context of geological disposal of radioactive waste. Review and Synthesis. NEA report Nr 6184
- Bonnet-Eymard T, Ceccaldi F, Richard L (2011) Extension of the Andra underground laboratory: methods and equipment used for dry, dust-free works, in World Tunnel Congress 2011, Helsinki
- Bossart P, Meier PM, Moeri A, Trick T, Mayor J-C (2002) Geological and hydraulic characterization of the excavation disturbed zone in the opalinus clay of the Mont Terri. *Eng Geol* 66:19–38
- Bourdarot G (1996) Essais de puits: méthodes d'interprétation. Éditions Technip; Institut français du pétrole, Paris, p 350
- Davy CA, Skoczylas F, Barnichon J-D, Lebon P (2007) Permeability of macro-cracked argillite under confinement: gas and water testing. *Phys Chem Earth* 32:667–680
- Delay J, Vinsot A, Krieguer JM, Rebours H, Armand G (2007) Making of the underground scientific experimental programme at the Meuse/Haute Marne URL, North Eastern France. *Phys Chem Earth* 32:2–18
- Diederichs MS (2003) Rock fracture and collapse under low confinement conditions. *Rock Mech Rock Eng* 36(5):339–381
- Emsley S, Olsson O, Stenberg L, Alheid H-J, Falls S (1997) ZEDEX: a study of damage and disturbance from tunnel excavation by blasting and tunnel boring. Svensk Kärnbränslehantering AB/Swedish Nuclear Fuel and Waste Management Co
- Fairhurst C, Damjanac B (1996) The excavation damage zone an international perspective. In: Martino JB, Martin CD (eds) Proceedings of the EDZ Workshop. Canadian Nuclear Society, pp 3–14
- Fierz T, Piedevache M, Delay J, Armand G, Morel J (2007) Specialized instrumentation for hydromechanical measurements for hydromechanical measurements in deep argillaceous rock, FMGM 2007: Seventh International Symposium on Field Measurements in Geomechanics
- Horne RN (1997) Modern Well Test Analysis. A computer-aided approach. Petroway, Inc., p 257
- Lanyon B (2011) Excavation Damaged Zones Assessment, NWMO internal report DGR-TR-2011-21, p 95
- Martin CD, Lanyon GW, Blümling P, Mayor JC (2002) The excavation disturbed zone around a test tunnel in the Opalinus Clay. In: Hammah R, Baden W, Curran J, Telesnicki M (eds) Proceedings NARMS/TAC 2002, University of Toronto Press, Toronto, pp 1581–1588
- Martin F, Lavignerie R, Armand G (2010) Geotechnical feedback of the new galleries excavation at the ANDRA underground research laboratory—Bure (France), Eurock 2010, Lausanne
- Meier P, Trick TH, Blümling P, Volckaert G (2001) Self-healing of fractures within the EDZ at the Mont Terri Rock Laboratory: results after one year of experimental work. Hydromechanical and thermohydromechanical behaviour of deep argillaceous rock: Theory and experiments. In: Proceedings of the International Workshop on Geomechanics, Paris, 11–12 Oct 2000, pp 275–283
- Möri A, Bossart P (1999) Visualisation of Flow Paths (FM-B experiment). In: Thury, M., Bossart, P. (Eds), Results of the Hydrogeological, Geochemical and Geotechnical Experiments (performed in 1996 and 1997) Geological Report No 23. Swiss National Geological Survey and Hydrogeological Survey, Ittigen-Berne, pp 113–121
- Pickens JF, Grisak GE, Avis JD, Belanger DW, Thury M (1987) Analysis and interpretation of borehole hydraulic tests in deep boreholes: principles, model development, and applications. *Water Resour Res* 23(7):1341–1375
- Pusch R, Stanfors R (1992) The zone of disturbance around blasted tunnels at depth. *Int J Rock Mech Min Sci Geomech Abstr* 29(5):447–456
- Schuster K, Alheid H-J, Böddener D (2001) Seismic investigation of the EDZ in opalinus clay. *Eng Geol* 61:189–197
- Tauzin E, Johns RT (1997) A new borehole simulator for well test analysis in low permeability formations. In: Proceedings of the IAMG'97 the annual conference of the international association for mathematical geology, Barcelona
- Tsang CF, Bernier F, Davies C (2005) Geohydromechanical processes in the excavation damaged zone in crystalline rock, rock salt, and indurated and plastic clays—in the context of radioactive waste disposal. *Int J Rock Mech Min Sci* 42(1): 109–125
- Wileveau Y, Bernier F (2008) Similarities in the Hydro-Mechanical response of Callovo-Oxfordian clay and Boom Clay during gallery excavation. *Phys Chem Earth* 33:S343–S349
- Wileveau Y, Cornet FH, Desroches J, Blümling P (2007) Complete in situ stress determination in an argillite sedimentary formation. *Phys Chem Earth* 32:866–878